Journal of The Electrochemical Society

OPEN ACCESS

Electrochemistry of Cu_xSi_{1-x} Alloys in Li Cells

Electrochemistry of Cu_xSi_{1-x} Alloys in Li Cells

Zhijia Du,[a] Hui Liu,[b,c] S. N. Ellis,[b] R. A. Dunlap,[a,d,e] M. Zhu,[c] and M. N. Obrovac[a,b,d,*,z]

[a]*Department of Physics and Atmospheric Science, Dalhousie University, Halifax, Nova Scotia B3H 4R2, Canada*
[b]*Department of Chemistry, Dalhousie University, Dalhousie University, Halifax, Nova Scotia B3H 4R2, Canada*
[c]*School of Material Science and Engineering, South China University of Technology, Guangzhou, Guangdong 510640, People's Republic of China*
[d]*Institute for Research in Materials, Dalhousie University, Halifax, Nova Scotia B3H 4R2, Canada*
[e]*College of Sustainability, Dalhousie University, Halifax, Nova Scotia B3H 4R2, Canada*

The structure and electrochemistry in lithium cells of sputtered thin films and ball milled alloys in the Cu-Si system ($0 \leq x \leq 0.60$ in Cu_xSi_{1-x}) were investigated. Both thin films and ball milled Cu-Si alloys showed the co-existence of amorphous Si and a nanocrystalline Cu_3Si phase. The lithiation potential of Cu-Si alloys was found to be significantly shifted to potentials below that of pure Si. In addition, the Cu_3Si phase was found to be involved in the electrochemical reaction of the alloys with lithium, however not all of the Si could be reacted with Li to its full theoretical extent. This suggests that a ternary Cu-Li-Si phase may be formed at full lithiation of these alloys.

Manuscript submitted February 18, 2016; revised manuscript received April 8, 2016. Published April 20, 2016.

Silicon containing alloys are promising anode materials for Li-ion batteries.[1] This is because of the high volumetric capacity of Si (2194 Ah/L, including volume expansion), which is much higher than graphite (764 Ah/L),[2] commonly used in commercial cells. However, the high volume expansion of Si during lithiation can lead to poor cycle life from structural degradation. It has been shown that crystalline Si can be cycled stably with a limited capacity by using a lower cutoff potential of 170 mV.[3] Another way to improve the cycling performance of Si is by adding inactive compounds to form active/inactive Si alloys. The inclusion of inactive components in an active/inactive Si alloy dilutes the volume expansion and maximizes the energy density at a given volume expansion.[4] In recent publications,[5–8] it has been shown that the formation of the $Li_{15}Si_4$ phase can be avoided in active/inactive Si alloys even when these electrodes were cycled to 5 mV, leading to excellent cycling performance.

Various Si-based alloys have been studied as anode materials for Li-ion batteries, such as C-Si,[9,10] Cr-Si,[11] Fe-Si,[12,13] Ni-Si,[8,14] Ti-Si,[15,16] etc. The Cu-Si alloy system differs from other M-Si systems because it has no silicon-rich silicide phase. Furthermore, the Cu-Si system forms several Li-Cu-Si ternary phases according to Inorganic Crystal Structure Database (ICSD) and other recent reports,[17,18] while the Fe-Si, Co-Si, Cr-Si or Mn-Si alloy systems do not. Therefore, the electrochemical behavior of the Cu-Si system with lithium may be different from alloys of Si with other first-row transition metals. Cu-Si alloys have also been evaluated as possible anode candidates for Li-ion cells.[19–25] Kim et al. synthesized a carbon-coated Si-Cu_3Si-Cu composite by chemical reduction of Cu^{2+} in a Si powder suspension, followed by pyrolysis of polyvinyl alcohol.[20] The X-ray diffraction (XRD) pattern of a fully lithiated electrode suggested that Cu_3Si is inactive toward lithium. Ahn et al. sputtered a Cu-Si thin film, which was composed of Cu nano-dots uniformly distributed in an amorphous Si matrix.[23] The authors stated that Cu nano-dots could stabilize the amorphous Si electrodes resulting in good cyclability. However, these previous reports involved very few compositions and often produced very different capacities as a result of different preparation methods. To our knowledge, no relationship between composition and electrochemical performance of Cu-Si alloys has been reported.

In the present study, a systematic investigation of the Cu-Si system has been undertaken in order to assess their electrochemical behavior in Li cells. Cu_xSi_{1-x} alloys with x ranging from 0 to 0.6 were prepared by combinatorial sputtering and ball milling in order to evaluate the effects of both composition and preparation method on their electrochemical behavior.

Experimental

Thin film libraries of Cu_xSi_{1-x} alloys were fabricated using a modified Corona Vacuum System V3-T sputtering system as described previously.[26] The base pressure for sputtering was below 4×10^{-7} Torr. Ar gas flow maintained the pressure at 1.0 mTorr during sputtering. In total, two Cu_xSi_{1-x} libraries ($0 \leq x \leq 0.38$, $0.30 \leq x \leq 0.61$) were prepared using a constant mask for the Si target, a linear-out mask for one Cu target, and a constant mask for a second Cu target. Sputtering substrates were a Si wafer (for X-ray diffraction studies), Ni foil (for compositional studies) and Cu discs (for weight measurements and electrochemical cells). Powder-based Cu_xSi_{1-x} alloys ($x = 0$, 0.05, 0.1, 0.2, 0.3, 0.4, 0.5 and 0.6) were prepared by the mechanical milling of stoichiometric amounts of Cu powder (Aldrich, −325 mesh, powder, dendritic, 99.7%) and Si powder (Sigma-Aldrich, −325 mesh, 99%) in an argon atmosphere using procedures as described previously.[8]

The position dependence of the mass for sputtered thin films was determined by the weighing of Cu discs before and after sputtering using a Sartorius SE-2 microbalance (±0.1 μg resolution). Composition data were collected using a JEOL 8200 microprobe from measurements of samples sputtered on a Ni foil. X-ray diffraction (XRD) measurements of samples sputter deposited on Si wafers were made using a Bruker D-8 Discover diffractometer equipped with a Vantec-2000 area detector and a Cu target X-ray tube. X-ray diffraction patterns of powder-based Cu_xSi_{1-x} alloys were collected using a JD2000 diffractometer equipped with a Cu K_α X-ray source and a diffracted beam monochromator. True densities of the samples were measured using a Micromeritics AccuPyc II 1340 gas pycnometer.

For powder-based alloys, slurries were made by mixing Cu_xSi_{1-x} alloys, carbon black (from Super P, Erachem Europe) and a 10 weight% aqueous solution of lithium polyacrylate (LiPAA) with a volumetric ratio of 80/5/15 in distilled water. The coatings were then dried in air at 120°C for 1 hour.

Electrodes were punched into discs with 1.27 cm diameter and dried at 100°C under vacuum before cell assembly. 2325-type coin cells were assembled with lithium foils as counter / reference electrodes and Celgard 2300 was used as the separator. The electrolyte was 1 M $LiPF_6$ (BASF) in a solution of ethylene carbonate, diethyl carbonate and monofluoroethylene carbonate (volume ratio 3:6:1, all from BASF). Cells were cycled at 30.0 ± 0.1°C between 5 mV–0.9 V

*Electrochemical Society Member.
[z]E-mail: mnobrovac@dal.ca

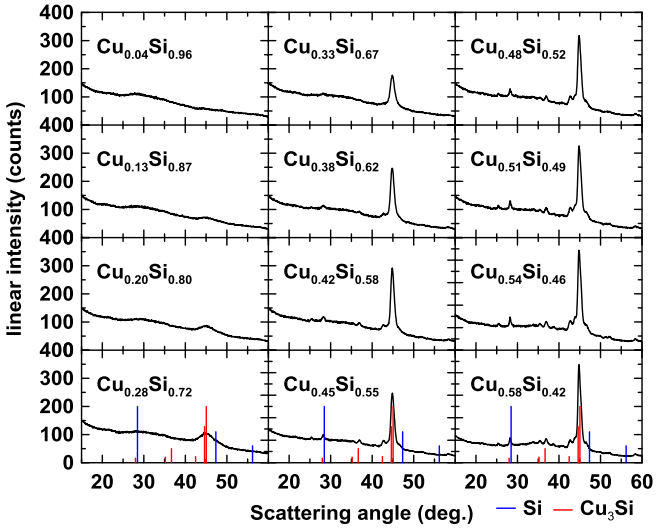

Figure 1. Selected XRD patterns of Cu_xSi_{1-x} thin films sputtered on Si wafers. The composition of each film is indicated in the figure. Diffraction peaks for Si and Cu_3Si are shown by blue and red lines, respectively.

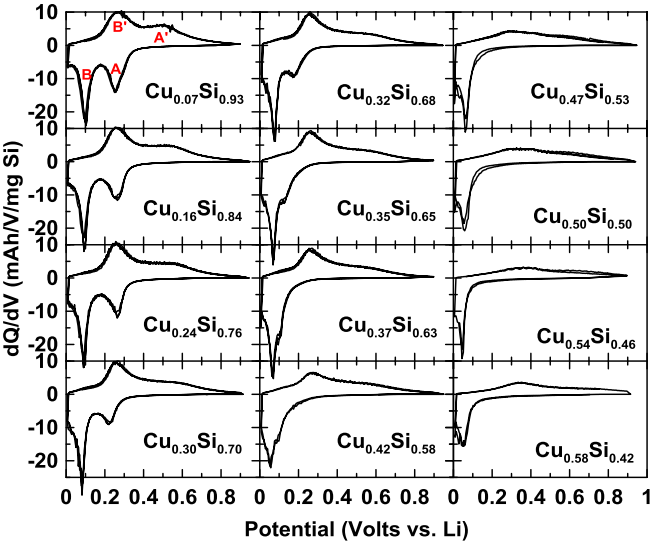

Figure 3. Differential capacity curves of Cu_xSi_{1-x} thin films for the cells shown in Figure 2.

with a Maccor Series 4000 Automated Test System at a constant current C/10 rate with a C/25 trickle discharge (lithiation).

Results

Figure 1 shows selected XRD patterns of sputtered Cu_xSi_{1-x} thin films. Thin films with high Si contents are completely amorphous. With increasing x (Cu content), peaks from the Cu_3Si phase appear with increasing peak intensity. No crystalline Si peaks are observed for any composition of the sputtered thin films. The microstructure of sputtered Cu-Si thin films appears to be different from other transition metal-Si systems with similar composition range as reported previously, where all compositions were fully amorphous/nanocrystalline.[7,12]

Figure 2 shows the potential vs. capacity profiles of selected Cu_xSi_{1-x} thin films. At high Si content, the potential vs. capacity curves show typical characteristics of amorphous Si with two sloping plateaus. With increasing x, the demarcation of the two sloping plateaus becomes less distinct. The sloping feature of these curves

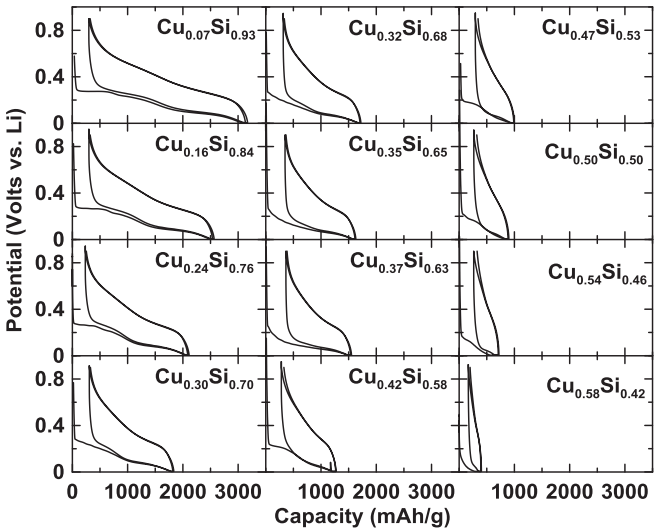

Figure 2. Potential versus capacity curves of Cu_xSi_{1-x} thin films with selected compositions.

indicates that the thin films remain amorphous/nanocrystalline during lithiation/delithiation and no $Li_{15}Si_4$ is formed during cycling.[3] The irreversible capacity of the first cycle remains nearly unchanged as a function of composition.

Differential capacity curves (dQ/dV) of Cu_xSi_{1-x} thin films as derived from Figure 2 are shown in Figure 3. The differential capacity curves of samples with high Si contents have two broad lithiation peaks (denoted as A and B) and two corresponding delithiation peaks (denoted as A′ and B′), which is typical of amorphous Si. With increasing x, both peaks A and B shift to lower potential, but peak A shifts more rapidly than peak B. The difference between the positions of peaks A and B gradually decreases and they merge into one peak at composition of $Cu_{0.42}Si_{0.58}$. At values of x above 0.42, this peak continues to shift to lower potential, but this is not possible to distinguish peak A and peak B. More will be discussed regarding this peak below. It is interesting that the behavior of peaks A and B with increasing x is different than for Ni-Si thin films, in which both peaks A and B are shifted by equal amounts with increasing Ni content.[7] This suggests that nanocrystalline Cu_3Si plays a role during lithiation, which results in these features in the differential capacity, that are not observed for other Si-M alloys, as discussed below. In contrast, during delithiation, two broad peaks, B′ and A′, have the same features as for pure amorphous Si, and little difference can be seen in differential capacity curves for $x \leq 0.35$. With further increase in x, the area of both peaks B′ and A′ decreases.

The changes in differential capacity result in marked changes in the average potential of the Cu_xSi_{1-x} thin film alloys with composition. Figure 4 shows the second lithiation average potential, the second delithiation average potential and total average cell polarization as a function of x. The data are divided into two regions. For thin films with $x \leq 0.35$ (Region I), the average lithiation potential decreases with increasing x while the average delithiation potential remains unchanged. This phenomenon has been recently found for sputtered Ni_xSi_{1-x} thin films with $x \leq 0.25$.[7] The depression of the lithiation potential is thought to originate from large internal stresses between the active phase and the inactive phases during volume expansion,[7] while the constant delithiation average potential with composition was thought to be a result of stress relief due to alloy fracturing under tensile stress.[27,28] In the case of Cu_xSi_{1-x} thin film alloys, the shift of peak A to lower potentials further contributes to the lowering in lithiation potential with x. Since the potential is lowered linearly with x, it is likely that peak A does indeed shift to values below 5 mV (the cutoff potential) at high values of x. This should result in a lowering in capacity, which will be confirmed below. When x

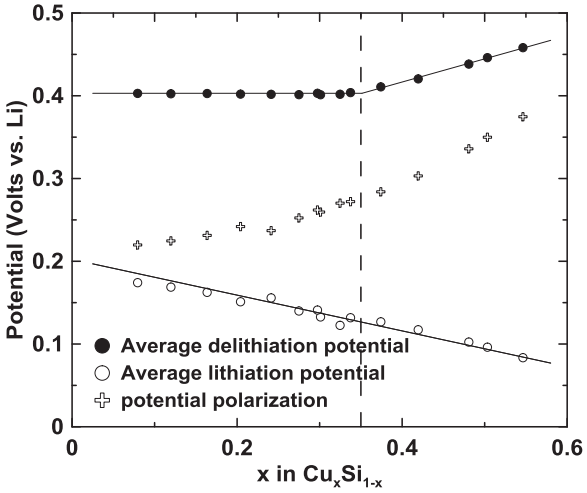

Figure 4. Second cycle average lithiation potential, average delithiation potential and polarization versus composition of sputtered Cu_xSi_{1-x} thin films.

in Cu_xSi_{1-x} is increased to values greater than 0.35 (Region II), the average delithiation potential begins to increase linearly. It can be observed that both peak B′ and A′ start to shift to higher potential. This might be ascribed to stress-potential coupling due to tensile stresses that could not be fully released by fracturing. In summary, as x is increased the average lithiation potential decreases due to stress from the inactive phase (causing both A and B peaks to shift) plus a chemical effect from the presence of Cu which causes the A peak to shift much more rapidly to lower potential than the B peak. During delithiation, the compressive stresses encountered during lithiation may not be fully released by fracturing, leading to an increase in charge potential with increasing Cu content.

Figure 5 shows the first reversible capacity of the Cu_xSi_{1-x} thin films as a function of x. The capacities are well below the theoretical line that assumes all the Si is active with a capacity of 3579 mAh/g. If Cu_3Si is taking part in the lithiation reaction, as suggested by the differential capacity, then evidently all the Si in this phase is not free to react with Li to its full extent. This suggests ternary phase formation may be occurring. Maranchi et al. have suggested that the ternary Cu_2LiSi phase forms in the interlayer between Si films and Cu, when such films are lithiated.[29] The formation of this phase at full lithiation fits the capacity trend we observed well, as shown by the dashed curve

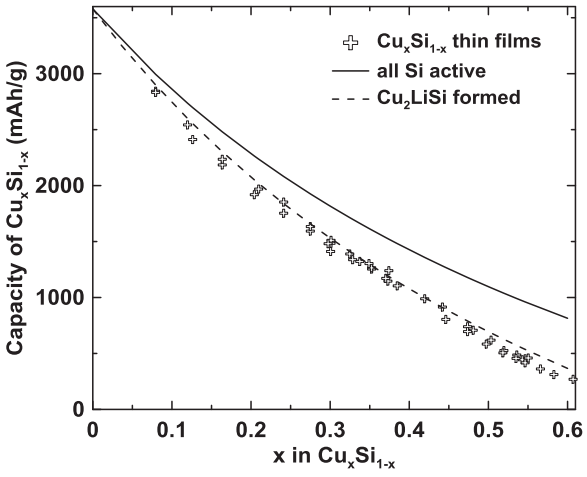

Figure 5. First cycle discharge and charge capacities of Cu_xSi_{1-x} thin films.

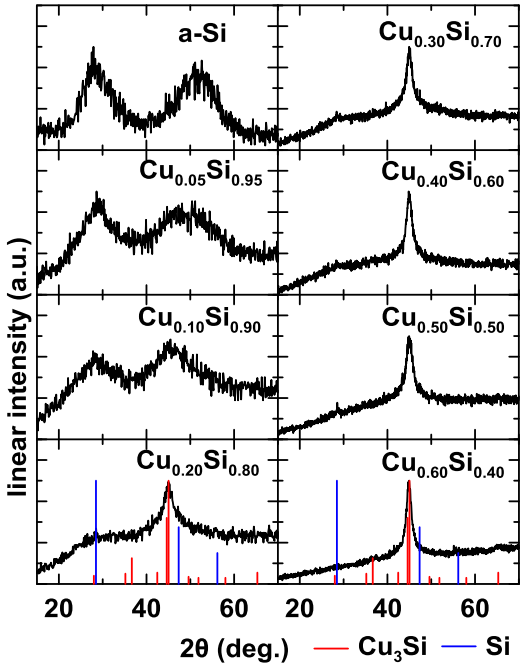

Figure 6. X-ray diffraction patterns of ball milled Cu_xSi_{1-x} alloys.

in Figure 5. Here the dashed curve is drawn according to the reaction:

$$\left(\frac{15}{4} - 22x\right) Li + \frac{x}{3} Cu_3Si + \left(1 - \frac{4x}{3}\right) Si \rightarrow \frac{x}{2} Cu_2LiSi + \frac{1}{4}\left(1 - \frac{3x}{2}\right) Li_{15}Si_4 \quad [1]$$

where the Cu_xSi_{1-x} films were assumed to be composed of a Cu_3Si/Si two-phase alloy, as suggested by XRD. At x values above about x = 0.42, the capacity becomes slightly lower than the dashed line. This is believed to be due to the truncation of the peak A as it shifts below 5 mV, as discussed above. Therefore the capacities of the thin film Cu_xSi_{1-x} alloys are consistent with the formation of the ternary Cu_2LiSi phase at full lithiation. Although the capacity trend is well explained by this reaction, a more detailed study is warranted to make final confirmation of the formation of the Cu_2LiSi phase.

Ball milled Cu-Si alloys were also prepared and studied in the present work in order to further elucidate the electrochemical properties of this system and its dependence on synthesis/sample microstructure. Figure 6 shows the XRD patterns of ball milled Cu_xSi_{1-x} powders. The XRD pattern of pure Si after ball milling has features characteristic of amorphous Si.[8] With increasing Cu content, the diffraction peak at about 45° gradually increases in intensity. This peak corresponds to the Cu_3Si phase (PDF No. 00-051-0916[17]) which has its two strongest diffraction peaks at 44.6° and 45.0°. The width of this peak indicates that the Cu_3Si phase formed during ball milling is nanocrystalline. These features and their dependence on composition are very similar to those observed for sputtered samples, shown in Figure 1.

Figure 7 shows the potential vs. capacity curves of ball milled Cu_xSi_{1-x} alloy electrodes for the first three cycles. The potential vs. capacity curves for all compositions have sloping plateaus, very similar to their sputtered thin-film counterparts. During the first discharge, all potential vs. capacity curves have a small plateau at about 0.6 V, which may be attributed to the presence of minor oxide impurities.[30] For lower values of x, two distinct sloping plateaus are observed during lithiation and delithiation that are characteristic of amorphous Si.

Figure 8 shows the first three, 20th and 50th differential curves of ball milled Cu-Si alloy electrodes. For Si-rich samples, two broad peaks (labeled A and B) during lithiation and two broad peaks (labeled

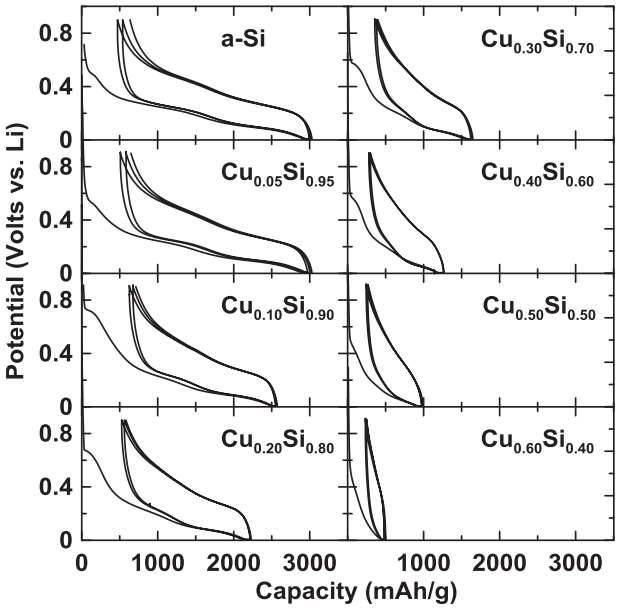

Figure 7. Potential versus capacity curves of ball milled Cu_xSi_{1-x} alloy electrodes.

B′ and A′) during delithiation are observed. With increasing x, peak A shifts to lower potential and decreases in area during lithiation. Peak B also shifts to lower potential at the same rate as peak A with increasing x and begins to truncate at 5 mV for $Cu_{0.60}Si_{0.40}$. This is different than the behavior of thin film Cu-Si alloys described above, where peak A shifted to a much greater extent than peak B. Instead, the shifting of the A and B peaks to lower potential with increasing Cu content in ball milled Cu-Si alloys is very similar to the behavior of ball milled Ni-Si alloys.[8] These effects are likely due to potential-stress coupling.[7]

The variation of the differential capacity curves during the delithiation of ball milled Cu-Si alloys is also very similar to that observed for the ball milled Ni-Si alloys. Ball milled Si shows a sharp peak at 0.42 V during delithiation at 20th cycle, which is typical for the transition from crystalline $Li_{15}Si_4$ to amorphous Si.[2] However, the exact reason why the amorphous ball milled Si does not go through the formation of $Li_{15}Si_4$ during the first several cycles is not clear. With the addition of 5 at% or more Cu in the alloy, no $Li_{15}Si_4$ is observed during lithiation/delithiation for 50 cycles. This is typical of previous results that show that Si alloys which include inactive compounds avoid the formation of $Li_{15}Si_4$ during lithiation due to lithiation potential depression by internal stress.[7,8]

Figure 9 shows the average lithiation and delithiation potential of the second cycle of ball milled Cu-Si alloys. The average potentials were fit by linear regression. The average potential of the x = 0.6 sample was not included in the fit, since the capacity of this alloy composition is so small that the contribution from carbon black is likely becoming dominant in this cell. The average lithiation potential is continuously depressed by increasing Cu content in the alloys, which is expected from stress-potential coupling induced by the inactive phase.[7,8] The delithiation potential increases with Cu content, presumably due to the analogous release of compressive stress during delithiation.

Figure 10 shows the first discharge and charge capacity of ball milled Cu_xSi_{1-x} alloys versus x. A low Coulombic efficiency for the first cycle is observed. The first lithiation capacity would tend to be larger than the theoretical capacity, since it would include Li consuming reactions involved in the formation of the solid electrolyte interphase (SEI). The first delithiation capacity, on the other hand, would tend to be lower than the theoretical capacity since the large volume expansion in some of these alloys would cause mechanical failure upon delithiation, resulting in electrical disconnection and capacity loss. Therefore the theoretical capacity is likely to reside somewhere

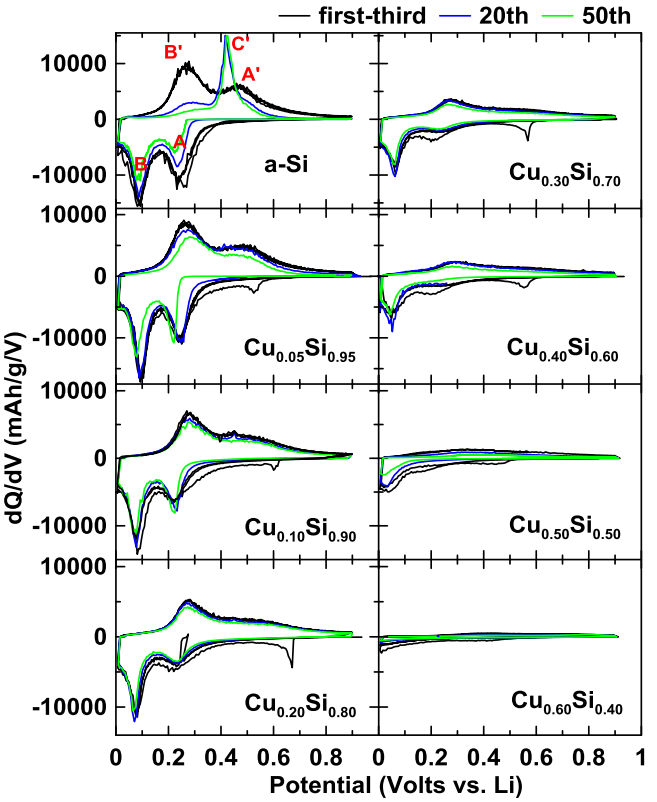

Figure 8. Second cycle average lithiation potential and average delithiation potential versus composition of ball milled Cu_xSi_{1-x} alloy samples. The average potentials were fit by linear regression. The average delithiation potential of the x = 0.6 sample was not included in the fits.

between the observed lithiated and delithiated capacity values. As the alloy capacity becomes smaller (larger Cu), the capacity and volume expansion should also become smaller and the delithiated capacity should approach the theoretical capacity. Also shown in Figure 10 is the theoretical capacity based on the formation of Cu_2LiSi at full lithiation (Equation 1). This line also fits the capacity trends well, falling between the observed cell first discharge and first charge capacities at

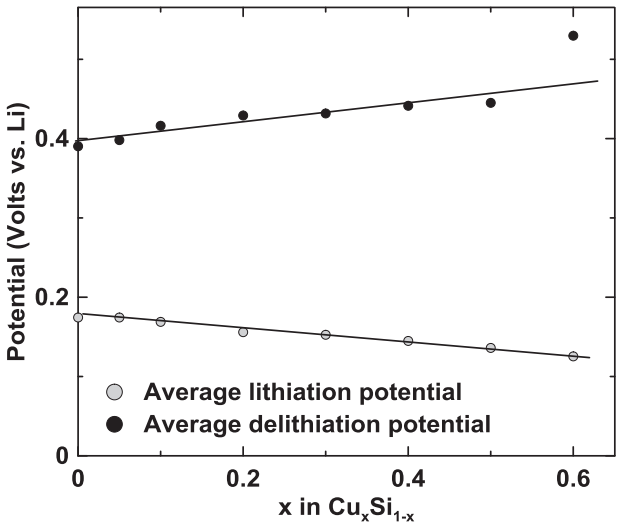

Figure 9. Differential capacity curves of ball milled Cu_xSi_{1-x} alloy electrodes for first-third cycles (black lines), 20th cycle (blue lines) and 50th cycle (green lines).

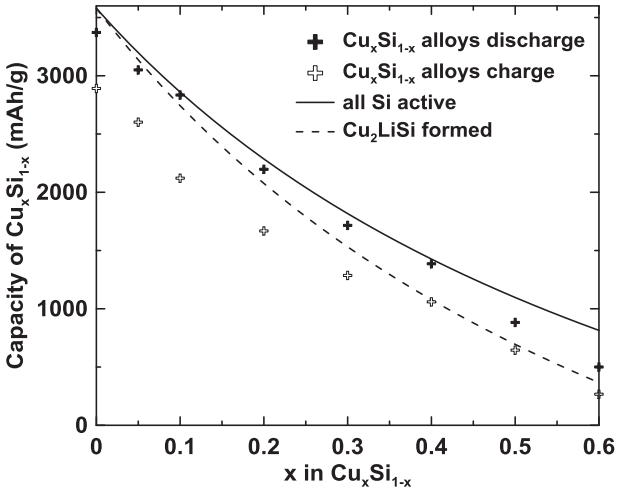

Figure 10. First cycle discharge and charge capacities for ball milled Cu_xSi_{1-x} alloys.

most alloy compositions and approaching the delithiation capacity at compositions with high Cu content.

Figure 11 shows the ex-situ XRD patterns of the $Cu_{0.40}Si_{0.60}$ sample before and after being discharged to 5 mV. It can be clearly seen that the Cu_3Si peak disappears after lithiation. New peaks were also formed in the XRD pattern of the lithiated sample. This demonstrates that Cu_3Si is also taking part in the lithiation reaction of ball milled Cu-Si alloys, and suggesting the formation of a ternary Cu-Li-Si ternary phase. We note that two of the largest peaks (around 31° and 44°) in the ex-situ XRD patterns are co-incident with the formation of Cu_2LiSi, which is also suggested by the capacity trend in Figure 10. However, a more detailed study is warranted to make final confirmation of the formation of the Cu_2LiSi phase.

Conclusions

Alloys in the Cu_xSi_{1-x} system with a composition range of $0 \leq x \leq 0.6$ have been prepared by both combinatorial sputtering and ball milling. These alloys were tested as anode materials for Li-ion batteries. The structure of all sputtered and ball milled samples showed features of amorphous Si and nanocrystalline Cu_3Si phase. The Cu_3Si phase was shown to take part in the electrochemical reaction with Li in both the Cu-Si sputtered films (by modification of the differential capacity) and in the Cu-Si ball milled alloys (by ex-situ XRD). In both cases the observed capacities were well below that expected if all the Si were free to react fully with Li. This suggests the formation of a ternary Cu-Li-Si phase during lithiation. It was found that the formation of Cu_2LiSi ternary alloy at full lithiation fit the observed capacity of all alloys well. The formation of this phase during the lithiation of Cu-Si alloys requires further confirmation.

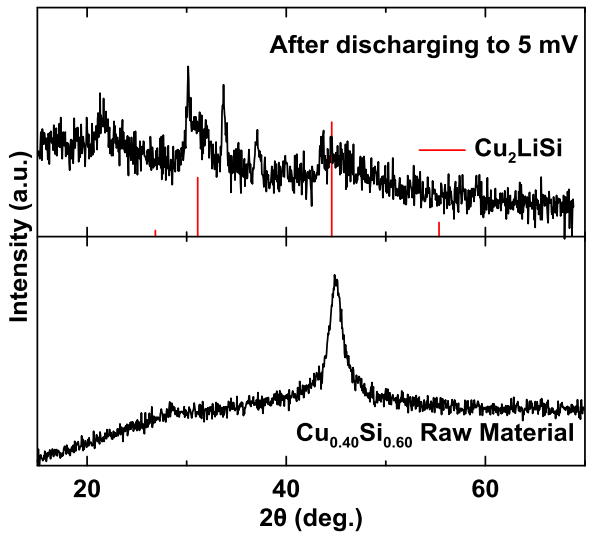

Figure 11. Ex-situ XRD pattern of ball milled $Cu_{0.40}Si_{0.60}$ before and after discharging to 5 mV. Red lines correspond to the diffraction peaks of crystalline Cu_2LiSi.

Acknowledgments

The authors acknowledge funding from NSERC and 3M Canada, Co. under the auspices of the Industrial Research Chair and Discovery grant programs. We also acknowledge the support of the Canada Foundation for Innovation, the Atlantic Innovation Fund and other partners that fund the Facilities for Materials Characterization managed by the Institute for Research in Materials. Zhijia Du acknowledges financial support from the Killam Trusts.

References

1. M. N. Obrovac and V. L. Chevrier, *Chem. Rev.*, **114** (23), 11444 (2014).
2. M. N. Obrovac and L. Christensen, *Electrochem. Solid-State Lett.*, **7**, A93 (2004).
3. M. N. Obrovac and L. J. Krause, *J. Electrochem. Soc.*, **154** (2), A103 (2007).
4. M. N. Obrovac, L. Christensen, Dinh Ba Le, and J. R. Dahn, *J. Electrochem. Soc.*, **154**, A849 (2007).
5. V. L. Chevrier, L. Liu, D. B. Le, J. Lund, B. Molla, K. Reimer, L. J. Krause, L. D. Jensen, E. Figgemeier, and K. W. Eberman, *J. Electrochem. Soc.*, **161**, A783 (2014).
6. Z. Du, R. A. Dunlap, and M. N. Obrovac, *J. Electrochem. Soc.*, **161**, A1698 (2014).
7. Z. Du, T. D. Hatchard, R. A. Dunlap, and M. N. Obrovac, *J. Electrochem. Soc.* **162**, A1858 (2015).
8. Z. Du, S. N. Ellis, R. A. Dunlap, and M. N. Obrovac, *J. Electrochem. Soc.* **163**, A13 (2015).
9. C. S. Wang, G. T. Wu, X. B. Zhang, Z. F. Qi, and W. Z. Li, *J. Electrochem. Soc.*, **145** (8), 2751 (1998).
10. A. Timmons, A. D. W. Todd, S. D. Mead, G. H. Carey, R. J. Sanderson, R. E. Mar, and J. R. Dahn, *J. Electrochem. Soc.*, **154** (9), A865 (2007).
11. W. J. Weydanz, M. Wohlfahrt-Mehrens, and R. A. Huggins, *J. Power Sources*, **81–82**, 237 (1999).
12. M. D. Fleischauer, J. M. Topple, and J. R. Dahn, *Electrochem. Solid-State Lett.*, **8** (2), A137 (2005).
13. G. X. Wang, L. Sun, D. H. Bradhurst, S. Zhong, S. X. Dou, and H. K. Liu, *J. Power Sources*, **88** (2), 278 (2000).
14. M.-S. Park, Y.-J. Lee, S. Rajendran, M.-S. Song, H.-S. Kim, and J.-Y. Lee, *Electrochim. Acta*, **50** (28), 5561 (2005).
15. Y.-S. Lee, J.-H. Lee, Y.-W. Kim, Y.-K. Sun, and S.-M. Lee, *Electrochim. Acta*, **52** (4), 1523 (2006).
16. K.-M. Lee, Y.-S. Lee, Y.-W. Kim, Y.-K. Sun, and S.-M. Lee, *J. Alloys Compd.*, **472** (1–2), 461 (2009).
17. International Centre for Diffraction Data PDF-2, Release 2002.
18. A. Slabon, S. Budnyk, E. Cuervo-Reyes, M. Wörle, C. Mensing, and R. Nesper, *Angew. Chem. Int. Ed.*, **51** (46), 11594 (2012).
19. B.-C. Kim, H. Uono, T. Satou, T. Fuse, T. Ishihara, M. Ue, and M. Senna, *J. Electrochem. Soc.*, **152** (3), A523 (2005).
20. J.-H. Kim, H. Kim, and H.-J. Sohn, *Electrochem. Comm.*, **7** (5), 557 (2005).
21. S. Yoon, S.-I. Lee, H. Kim, and H.-J. Sohn, *J. Power Sources*, **161** (2), 1319 (2006).
22. Y. NuLi, B. Wang, J. Yang, X. Yuan, and Z. Ma, *J. Power Sources*, **153** (2), 371 (2006).
23. H.-J. Ahn, Y.-S. Kim, W. B. Kim, Y.-E. Sung, and T.-Y. Seong, *J. Power Sources*, **163** (1), 211 (2006).
24. P. Zuo, G. Yin, X. Hao, Z. Yang, Y. Ma, and Z. Gao, *Mater. Chem. Phys.*, **104** (2–3), 444 (2007).
25. Y.-M. Kang, M.-S. Park, J.-Y. Lee, and H.-K. Liu, *Carbon*, **45** (10), 1928 (2007).
26. J. R. Dahn, S. Trussler, T. D. Hatchard, A. Bonakdarpour, J. N. Meuller-Neuhaus, K. C. Hewitt, and M. Fleischauer, *Chem. Mater.*, **14**, 3519 (2002).
27. V. A. Sethuraman, V. Srinivasan, A. F. Bower, and P. R. Guduru, *J. Electrochem. Soc.*, **157**, A1253 (2010).
28. D. S. M. Iaboni and M. N. Obrovac, *J. Electrochem. Soc.*, **163** (2), A255 (2016).
29. J. P. Maranchi, A. F. Hepp, A. G. Evans, N. T. Nuhfer, and P. N. Kumta, *J. Electrochem. Soc.*, **153** (6), A1246 (2006).
30. M. Miyachi, H. Yamamoto, H. Kawai, T. Ohta, and M. Shirakata, *J. Electrochem. Soc.*, **152**, A2089 (2005).